

# Experimental Study of Focused Ultrasonic Beams Reflected at a Fluid–Solid Interface in the Neighborhood of the Rayleigh Angle

Theodore E. Matikas, *Member, IEEE*, Martine Rousseau, and Philippe Gatignol

**Abstract**—An experimental technique is developed to measure the pressure field of an ultrasonic focused beam reflected from a water–aluminum interface. This experimental procedure, based on the cartography of the reflected beam, is used to demonstrate nonspecular phenomena at a range of angles of incidence near and at the Rayleigh angle. In particular, the lateral and axial displacements of the reflected focal point are quantified. The experimental results confirm previous theoretical work.

## I. INTRODUCTION

IN NONDESTRUCTIVE testing of materials, the experimenters use focused transducers in order to limit the diffusion effects which can be considerable particularly in metals. The quantitative study of the reflected beam is essential to obtain the correct interpretation of errors in measurements. Bertoni *et al.* [1] have studied the reflection of convergent beams at a liquid–solid interface for incidence at the Rayleigh angle. In their model they used the hypothesis of a well collimated beam. The approximate expression of the reflected acoustic field led to a direct integration. They obtained the position of the focal point of the reflected beam and predicted a lateral and axial displacement (there is no notion of a beam caustic).

In 1986, Nagy, Cho, Adler, and Chimenti [2] verified the axial displacement by means of schlieren photography.

In a recent article [3], we studied the reflection of an acoustic beam emitted by a model of a Gaussian focused transducer at a fluid–solid interface. The distribution of normal velocity was given on the emitting plane placed in the fluid medium. We introduced the notion of the caustic of the reflected beam. A distortion of this caustic was observed in the neighborhood of the Rayleigh angle, including a lateral and axial displacement of the focal point of the beam. Moreover, other nonspecular phenomena were predicted (spreading of the reflected beam,

asymmetric variation of the acoustic pressure around the axis, curvature of the acoustic axis). An analytical expression for the reflected field was then obtained by means of asymptotical methods (stationary phase, Ludwig method) based on the short wave hypothesis. This detailed analysis was completed with a physical interpretation of nonspecular phenomena and a comparison between nonspecular reflection of a focused and a parallel beam.

In the present work we propose a technique for measuring the lateral and axial displacements of the focal point, together with a qualitative representation of other nonspecular phenomena, based on the cartography of the reflected beam. A study of the feasibility of the experiment and the choice of the transducer is carried out. The results obtained are in agreement with our theoretical predictions [3].

## II. MATHEMATICAL FORMULATION

Consider a fluid–solid interface. The fluid is characterized by its mass density  $\rho_F$ , and the velocity of sound  $c$ , the elastic solid by its mass density  $\rho_S$ , the velocity of the longitudinal waves  $c_L$ , and the velocity of the transversal waves  $c_T$ . We refer to Fig. 1 for the definition of coordinates. The emitting plane is taken at  $z_i = 0$  in the fluid region. The incident angle is denoted by  $\Theta_I$ . The Gaussian normal velocity distribution along the plane of the transducer is given by

$$v_n(x_i, 0) = V_o e^{-\left(\frac{x_i}{a}\right)^2} e^{-ik \sin \theta_o \frac{x_i^2}{a}} e^{-i\omega t} \quad (1)$$

where  $V_o$  is the central magnitude of  $v_n$ ,  $a$  is the characteristic width of the Gaussian beam,  $k$  is the wavenumber in the fluid given by  $k = \omega/c$  (where  $\omega$  is the angular frequency of the emitter) and  $\theta_o$  is the half angle of convergent beam.

The pressure of the incident field is described by plane wave superposition in the form of a Fourier integral [4]:

$$p_{\text{inc}}(\bar{x}_i, \bar{z}_i) = \frac{\rho c V_o \sqrt{k a}}{2\sqrt{i\pi \sin \theta_o}} \int_{-\infty}^{+\infty} \frac{e^{-\left\{\frac{\bar{k}_x^2}{4 \sin^2 \theta_o}\right\}} e^{i(k a) f_i(\bar{k}_x)} d\bar{k}_x}{\bar{k}_{z_i}} \quad (2)$$

Manuscript received February 5, 1991; revised October 4, 1991; accepted May 15, 1992. This work was supported by the European Economic Community; General Division of Research, Industry and Development (DG XII) (program SCIENCE).

T. Matikas is with the U.S. Air Force Laboratories, Materials Directorate, WL/MLLP, Wright-Patterson Air Force Base, OH 45433-6533.

M. Rousseau is with the Laboratoire de Modelisation en Mecanique, CNRS (URA 229), Université Pierre et Marie Curie (Paris 6), Tour 66-4, Place Jussieu, 75252 Paris cedex 05, France.

P. Gatignol is with the Université de Technologie de Compiègne, Division Acoustique, B.P. 649, 60206 Compiègne cedex, France.

IEEE Log Number 9202168.

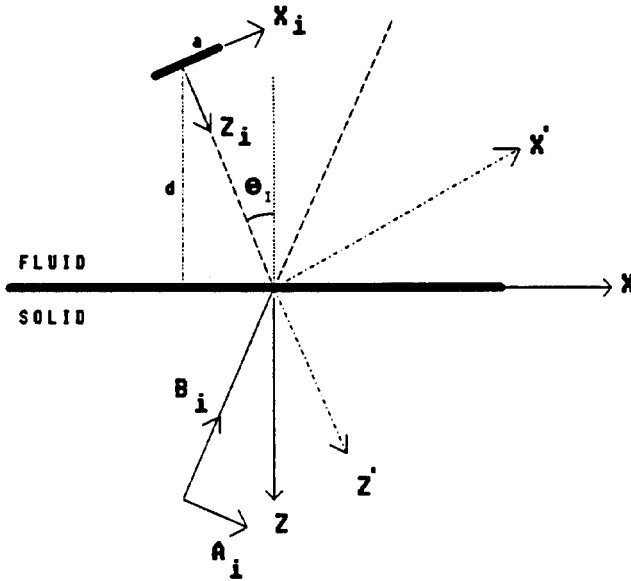


Fig. 1. Coordinate systems.  $(x_i, z_i)$  is the system linked to the emitter.  $(x, z)$  is the system linked to the interface, where the continuity conditions are written.  $(A_i, B_i)$  is the system linked to the reflected beam.  $(x', z')$  is the system where the reflected field is expressed (calculus system); the angle of incidence between the interface and  $x'$  axis is denoted  $\Theta_I$ .

where

$$f_i(\bar{k}_{x_i}) = \frac{\bar{k}_{x_i}^2}{4 \sin \theta_o} + \bar{x}_i \bar{k}_{x_i} + \bar{z}_i \bar{k}_{z_i} \quad (3)$$

with

$$\bar{k}_{z_i} = \sqrt{1 - \bar{k}_{x_i}^2}.$$

We introduced nondimensional parameters:

$$\bar{x}_i = \frac{x_i}{a}, \quad \bar{z}_i = \frac{z_i}{a}, \quad \bar{k}_{x_i} = \frac{k_{x_i}}{k}, \quad \bar{k}_{z_i} = \frac{k_{z_i}}{k}.$$

The pressure of the reflected field can be written as follows [3]:

$$p_{\text{ref}}(\bar{x}', \bar{z}') = \frac{\rho c V_o \sqrt{k a}}{2 \sqrt{i \pi \sin \theta_o}} \int_{-\infty}^{+\infty} R(\bar{k}_{x'}) \frac{e^{-\left\{ \frac{\bar{k}_{x'}^2}{4 \sin \theta_o} \right\}}}{\bar{k}_{z'}} e^{i(k a) f_r(\bar{k}_{z'})} d\bar{k}_{x'} \quad (4)$$

where

$$f_r(\bar{k}_{x'}) = \frac{\bar{k}_{x'}^2}{4 \sin \theta_o} + \bar{A}_i \bar{k}_{x'} + \bar{B}_i \bar{k}_{z'} \quad (5)$$

where  $\bar{A}_i = \bar{x}' \cos 2\theta_i + \bar{z}' \sin 2\theta_i$  and  $\bar{B}_i = \bar{x}' \cos 2\theta_i - \bar{z}' \sin 2\theta_i + (\bar{d}/\cos \theta_i)$ . The reflection coefficient of the fluid-solid interface, written in the system  $(x', z')$  is  $R(\bar{k}_{x'})$  and  $\bar{d} = d/a$ ; where  $d$  is the distance between the emitter and the interface (see Fig. 1).

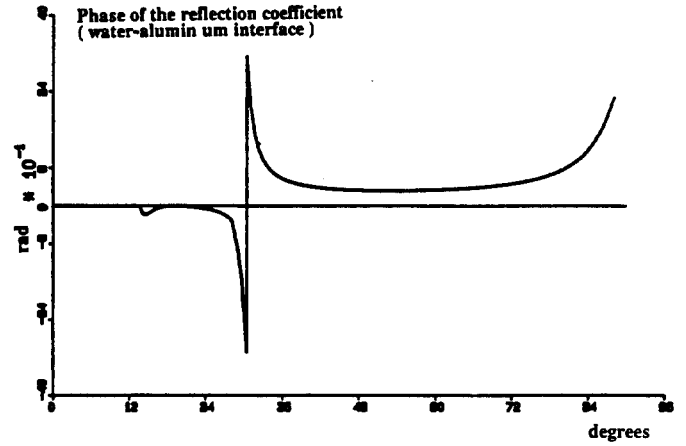


Fig. 2. Phase of the reflection coefficient (water-aluminum interface).

Two cases appear.

1) Case of an incidence far from the Rayleigh angle ( $\Theta_R$ ):

$$|\Theta_I - \Theta_R| > 1/ka.$$

The vanishing of the first and second derivative of the function  $f_r$ , results in the equation of the caustic of the reflected beam:

$$\bar{A}_i^{2/3} + \bar{B}_i^{2/3} = \left( \frac{1}{2 \sin \theta_o} \right)^{2/3}. \quad (6)$$

The vanishing of the first, second and third derivative,  $f_r' = f_r'' = f_r''' = 0$ , results in the position of the focal point:

$$\begin{aligned} A_i &= 0 \\ B_i &= 1/2 \sin \theta_o. \end{aligned} \quad (7)$$

This result for  $P_{\text{ref}}$  corresponds to that of the geometrical acoustics.

2) Case of an incidence in the neighborhood of the Rayleigh angle:

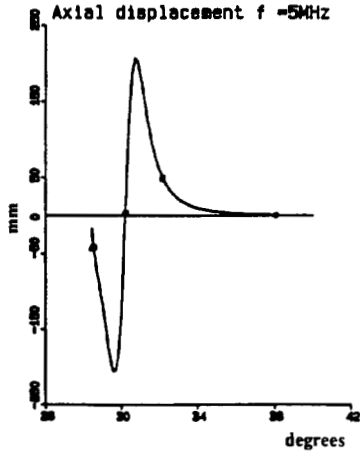
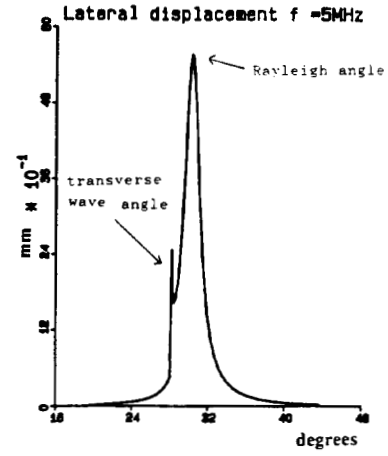
$$|\Theta_I - \Theta_R| < 1/ka.$$

As discussed in detail in [3], the reflection coefficient is approximated by expanding the amplitude and phase, and the reflected pressure integral (4) may be split up into three integrals in the neighborhood of each real saddle-point  $\gamma_i$  of the function  $f_r$  (stationary phase method).

Thus, the phase of the reflection coefficient,  $\varphi(\bar{k}_{x'})$ , which varies rapidly in the neighborhood of the Rayleigh incidence (see Fig. 2), may be expanded about the real saddle-points  $\gamma_i$  and the function  $f_r'$  becomes

$$\hat{f}_r'(\bar{k}_{x'}) = f_r'(\bar{k}_{x'}) + \frac{\frac{1}{n} \sum_{i=1}^n \{(\varphi'(\gamma_i) + \varphi''(\gamma_i))(\bar{k}_{x'} - \gamma_i)\}}{ka} \quad (8)$$

with  $n = 1$  or  $n = 3$ .


 Fig. 3. Axial displacement of the focal point ( $f = 5$  MHz).

 Fig. 4. Lateral displacement of the focal point ( $f = 5$  MHz).

Making use of the conditions  $\hat{f}'_r = \hat{f}''_r = \hat{f}'''_r = 0$ , we obtain the new position of the focal point as

$$\begin{cases} \bar{A}_i = \frac{1}{n} \sum_{i=1}^n \frac{\{\varphi'(\gamma_i) - \gamma_i \varphi''(\gamma_i)\}}{ka} \\ \bar{B}_i = \frac{1}{2 \sin \theta_o} + \frac{1}{n} \sum_{i=1}^n \frac{\varphi''(\gamma_i)}{ka} \end{cases} \quad (9)$$

In the case of an incidence near the Rayleigh angle, three saddle-points are in the neighborhood of zero. By comparing the expressions (7) and (9), we deduce the lateral,  $L$ , and axial,  $A$ , displacements of the focal point:

$$L = -\frac{\varphi'(0)}{ka} \quad \text{and} \quad A = \frac{\varphi''(0)}{ka} \quad (10)$$

where

$$\begin{cases} \varphi'(0) = \tilde{\varphi}'(\bar{k}_I) \cos \theta_I \\ \varphi''(0) = \tilde{\varphi}''(\bar{k}_I) \cos^2 \theta_I - \tilde{\varphi}'(\bar{k}_I) \sin \theta_I \end{cases} \quad (11)$$

Functions  $\varphi'(0)$  and  $\varphi''(0)$  are the first and second derivatives of the phase of the reflection coefficient, computed at the point zero in the system  $(x', z')$ , and  $\varphi'(\bar{k}_i)$  and  $\varphi''(\bar{k}_i)$  are the first and second derivatives, computed at the point  $\bar{k}_1 = \sin \theta_1$  in the system  $(x, z)$ .

The expressions (10) show that  $L$  and  $A$  are inversely dependent on frequency,  $f$ , of the emitter-transducer ( $k = 2\pi f/c$ ). In Figs. 3 and 4, we show the variation of the lateral and axial shifts of the focal point depending on the angle of incidence for a frequency of emission of 5MHz. Points in Fig. 3 correspond to the incidences: 28.5°, 30.5°, 32.5°, 38°, chosen for the experiments.

Finally, in Fig. 5 (extract of the [3]) we show our theoretical conclusions concerning nonspecular reflection in the case of an incidence near the Rayleigh angle.

The modified parts of the beam are: 1) lateral and axial displacements in a region around the focal point; 2) distortion of the caustic, spreading of the reflected beam, asymmetric variation of the acoustic pressure around the reflected caustic near the focal point; and 3) curvature of the acoustic axis along its entire length.

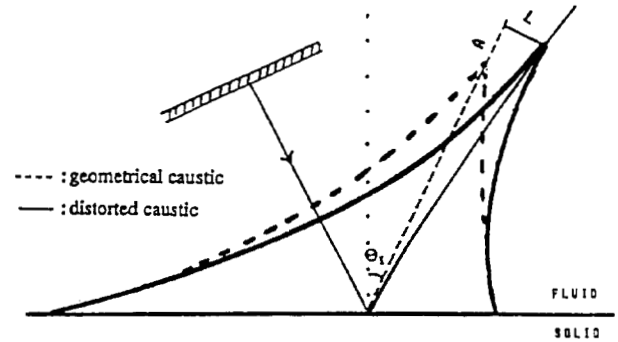


Fig. 5. Qualitative representation of the distortion of the reflected caustic.

### III. PRESENTATION OF THE EXPERIMENTAL DEVICE TECHNIQUE OF THE EXPERIMENT

We refer to Figs. 6 and 7 for the experimental setup that consists of a tank filled with water, at the bottom of which a piece of aluminum shaped according to Fig. 7, is immersed. The slope of the piece of aluminum is denoted  $\Theta_I$  and it corresponds to the angle of incidence of the beam. We used four pieces of aluminum with different slopes:  $\Theta_I = 28.5^\circ$ ,  $\Theta_I = 32.5^\circ$ ,  $\Theta_I = 38^\circ$ ,  $\Theta_I = \Theta_R = 30.5^\circ$  (Rayleigh angle for aluminum). The Rayleigh angle is calculated from the formula:

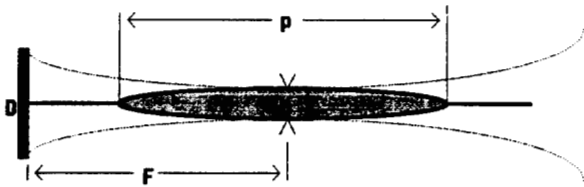
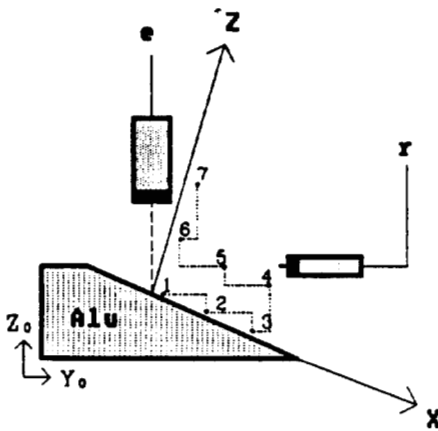
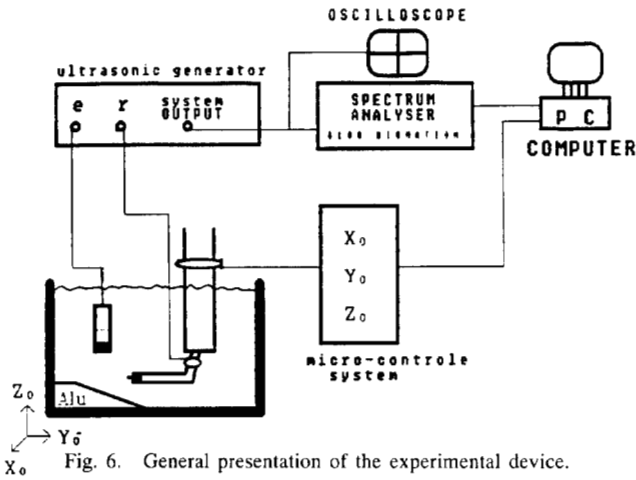
$$\theta_R = \alpha \sin \left( \frac{c}{\xi c_T} \right) \quad (12)$$

where  $\xi$  satisfies the equation:

$$\xi^6 - 8\xi^4 + 8\xi^2 \left( 3 - 2\frac{c_T^2}{c_L^2} \right) - 16 \left( 1 - \frac{c_T^2}{c_L^2} \right) = 0 \quad (13)$$

with  $c = 1480$  m/s,  $c_L = 6300$  m/s, and  $c_T = 3120$  m/s for aluminum.

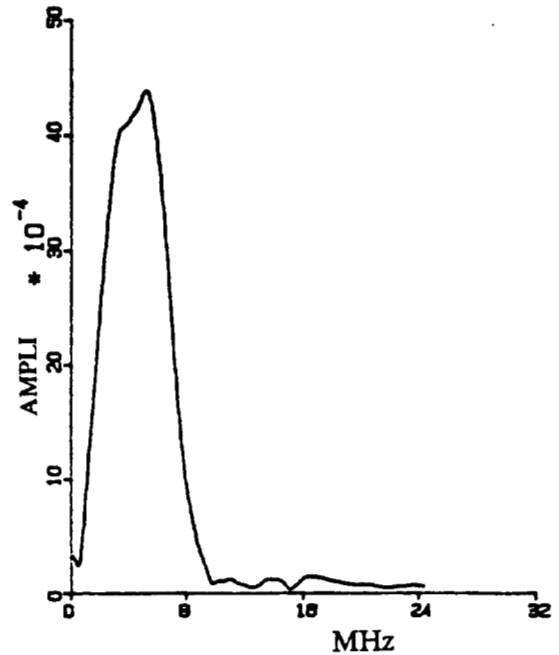
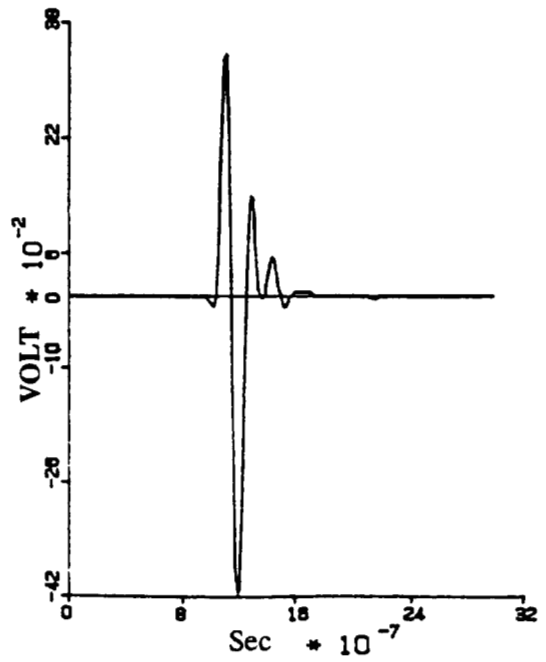
The emission part (e), contains a 5-MHz focused transducer placed on a microcontrol table manipulated following the three dimensions of the water tank. Initially, the transducer is placed above the horizontal side of the piece of aluminum. After ensuring the verticality of the emitted beam to the horizontal side, we measure the focal distance of the emitter, which is defined as the distance between the emission-reception side of



the probe, and the point of maximum acoustic pressure. The transducer is then displaced along the direction  $Y_0$ , and it is positioned above the sloped side of the piece of aluminum. By displacing it along the direction  $Z_0$ , we can vary the distance between the emitter and the interface (see Fig. 7).

In order that the lateral shift,  $L$ , of the focal point may be detected, the width of the focal spot,  $Q$ , must satisfy:  $Q < 2L$ . The theoretical results of Section II, show that the lateral displacement for incidence of the Rayleigh angle ( $30.5^\circ$ ) is 5.7 mm, for a transducer of 5-MHz frequency.

The focal spot is defined by all the points where the acoustic pressure is greater than a given value; this value being a fraction of the maximum value attained at the focal point. In practice, this fraction is taken to be one half (drop in acoustic pressure of 6 dB). For a focused probe having an axis of rotation symmetry, the focal spot appears as an ellipsoid elongated in the direction of the wave propagation (see Fig. 8).



The (14) and (15) give the length,  $P$ , and the width,  $Q$ , of the focal spot depending on the focal distance,  $F$ , the diameter of the transducer,  $D$ , and the wavelength,  $\lambda$ , of the acoustic waves:

$$P = 8.6\lambda(F/D)^2 \quad (14)$$

$$Q = 1.4\lambda F/D. \quad (15)$$

For our experiment, we chose a focused transducer type V 308 SU, having diameter of the active element of 19 mm, focal distance of 76.2 mm, and resonance frequency 5MHz. In

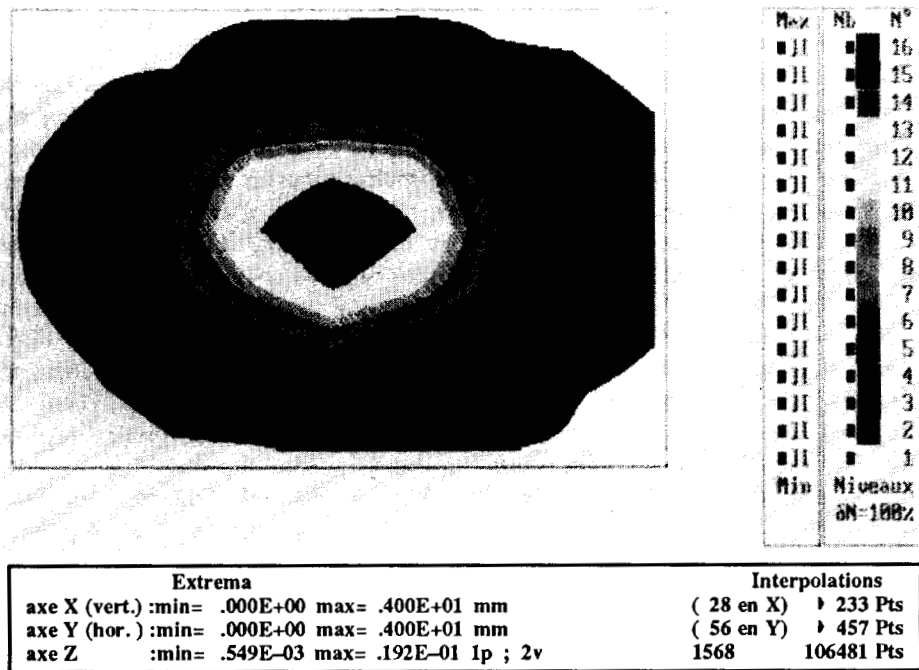


Fig. 11. Width of the focal spot.

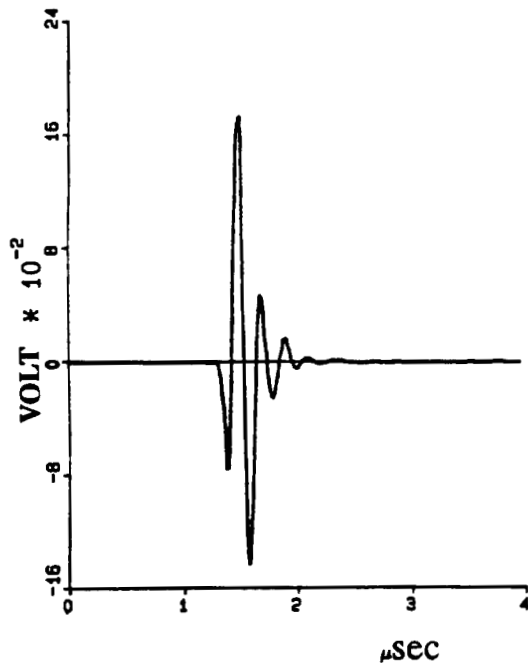


Fig. 12. Time signal.

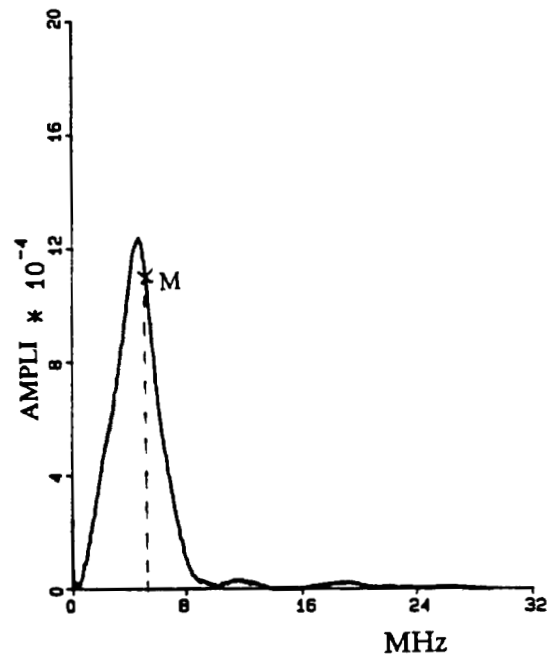


Fig. 13. Signal power spectrum.

Figs. 9 and 10 respectively, we represent the time and spectral responses of the transducer.

The experimental measure of the width of the focal spot is carried out by means of beam cartography. This technique is represented in Section IV.

Fig. 11 shows the measured profiles of the acoustic pressure in the focal plane of the emitter. The focal point is indicated by the level at the top of the scale. A drop of 6 dB corresponds to the eight highest levels in this scale. Thus we deduce the width of the experimental focal spot to be  $1.65 \pm 0.10$

mm. The convergence angle is  $F = \alpha \tan(Q/2F)$  or about  $0.6^\circ$ .

The detector contains a miniature probe. We use this probe as a wide-band point receiver to investigate the propagation in water of short pulses from the emitter transducer. The diameter and the thickness of the active element of the probe are 0.3 and 1.5 mm, respectively. The dimensions of the element give a probe capacitance of less than 50 pF and a head amplifier is normally required to avoid capacitive potential division in connecting cables.

This transducer-receiver is linked to a microcontrol system controlled by PC computer. Thus the miniature probe can be moved in three directions:  $X_o$ ,  $Y_o$ ,  $Z_o$ . We note that the accuracy of displacement is 0.1 mm for  $X_o$  and  $Y_o$  and 0.01 mm for  $Z_o$ . Automatic scanning enables the probe to carry out a displacement consisting of one movement along  $Y_o$ , thence along  $Z_o$ , in such a way that the global displacement remains parallel to the surface of the piece of aluminum (see Fig. 7). The positioning points of the probe (numbered in Fig. 7 as example) correspond to the digitization points. The ultrasonic generator used, was a Panametrics 5052 UA. The signal received was filtered through a "high pass" filter of 300 KHz, thence digitized by means of a spectrum analyzer (BIOMATION-8100) of a 100 MHz maximum frequency. Once digitized (quantification level 8 bites), the signal was windowed on 2048 points, then saved in the form of a file on the hard disk of the PC.

This experimental process presents certain advantages for the accuracy of the results: 1) The beam verticality with respect to the bottom of the tank being ensured (on the horizontal face of the aluminum pieces), the shape of these pieces enables us to determine the angle of incidence of the beam (which corresponds to the slope) with great precision; 2) precision of the position of the geometrical focal point (deduced by the geometry of the aluminum pieces); 3) the plan of the digitized signal points (denoted  $xz$ ) corresponds to the plan  $Y_oZ_o$  (because of the geometry of the aluminum pieces); and 4) during the displacement of the receptor-probe the system stocks the digitized signal of the preceding point. The digitization is carried out once the detector is fixed, thus an average of the signal may be computed.

#### IV. PROCESSING OF THE FILE CONTAINING THE DIGITIZED SIGNALS

To each point in the plane  $(x, z)$  containing the reflected beam (numbered in Fig. 7 as example) corresponds a time signal (see Fig. 12).

In order to determine the focal point of the reflected beam and to evaluate the lateral and axial shifts, we carry out successively a Fast Fourier transform (FFT) thence a computation of the amplitude,  $M$ , of the signal at the 5-MHz emitting frequency (see Fig. 13). A program enables us to go from the initial file of three variables (two spatial variables:  $x$ ,  $z$  and time) and one parameter (the amplitude of the signal depending on time), to an output file of two variables (spatial:  $x$  and  $z$ ) and one parameter (amplitude  $M$  of the signal at 5 MHz).

Figs. 14 to 17 represent the trace by isolevels of the output file, for different angles of incidence. Thus we obtain the cartography of the reflected field for the chosen frequency (5 MHz).

Following these figures, we obtain the coordinates of the focal point with respect to the origin  $O$  corresponding to the first point of digitalization (point 1 in Fig. 7). The positioning of this point is imposed by the experiment. We can then locate the focal point, and deduce a possible displacement

in respect to its position in the case of geometric acoustics.

Fig. 14 represents the reflected field for an angle of incidence of  $38^\circ$  (far from the Rayleigh angle). We deduce no lateral or axial shift; this result corresponds to that of the geometric acoustics. Figs. 16 and 17 represent the reflected field for an angle of incidence of  $28.5^\circ$  and  $32.5^\circ$  respectively (in the neighborhood of the Rayleigh angle). We deduce a lateral shift of about 3 mm, and an axial one of  $-43$  mm and 45 mm respectively. Fig. 15 represents the reflected field for an angle of incidence of  $30.5^\circ$ , which corresponds to the Rayleigh angle. We deduce a lateral shift of about 5.5 mm; the axial shift is not significant. These quantitative results are in agreement with our theoretical predictions shown at Figs. 3 and 4.

For an angle of incidence equal to the Rayleigh angle ( $30.5^\circ$ ), the acoustic axis of the reflected beam displays a curvature. Moreover, the variation of pressure is much greater in the right part of the beam than in the left one. For incidences in the neighborhood of the Rayleigh angle ( $28.5^\circ$ ,  $32.5^\circ$ ), these phenomena are present but they are less significant. For an angle of incidence far from the Rayleigh angle ( $38^\circ$ ), the reflected pressure variation is perfectly symmetrical around the acoustic axis. The above quantitative and qualitative experimental results have validated our theoretical model [3].

#### V. CONCLUSION

In a previous paper [3], using asymptotic analysis for the reflection of focused ultrasonic beams from a liquid-solid interface, the following nonspecular phenomena were predicted in the neighborhood of the Rayleigh angle of incidence: spreading of the reflected beam, asymmetric variation of the acoustic pressure around the axis, curvature of the acoustic axis, distortion of the caustic of the reflected beam including lateral and axial displacements of the focal point of the beam.

In this paper, we verified experimentally all those nonspecular phenomena; the results are in agreement with our theoretical conclusions [3]. The lateral and axial displacements of the focal point were quantified. The technique employed is based on the cartography of the reflected beam, i.e., the variation of the reflected pressure at each point of the fluid medium. This precise technique has also been employed to characterize the emitter.

An interesting issue of this work may be the use of the focal shift for the detection of variations of the phase of the reflection coefficient: nondestructive testing of the material surfaces, detection of structure defects. The lateral displacement may be profitable for the detection of adhesive bond defects: adhesive defect may be modeled as a modification of boundary conditions between the layer of glue and the substrata; for a given incidence, the derivatives of the phase of the reflection coefficient calculated to the first interface fluid-metal, appear in the analytical expressions of the lateral shift. This work is currently in progress.

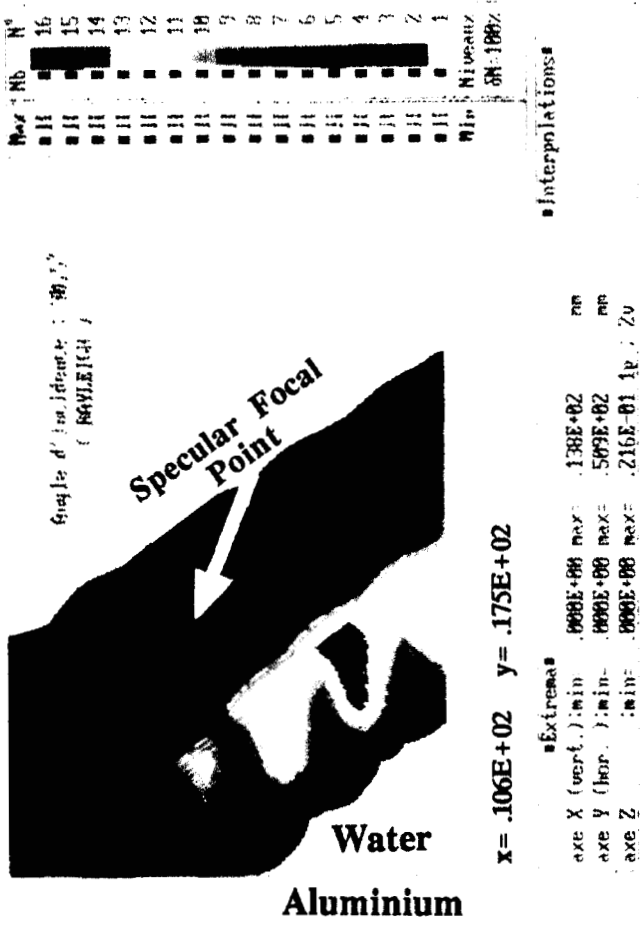


Fig. 15. Cartography of the reflected beam at 5 MHz; angle of incidence: 30.5°.

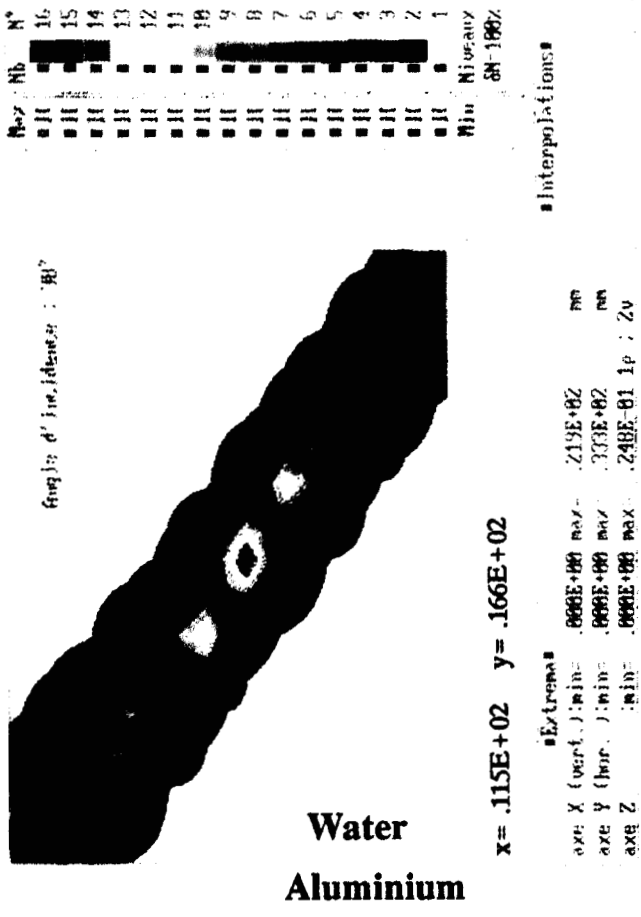


Fig. 14. Cartography of the reflected beam at 5 MHz; angle of incidence: 28.5°.

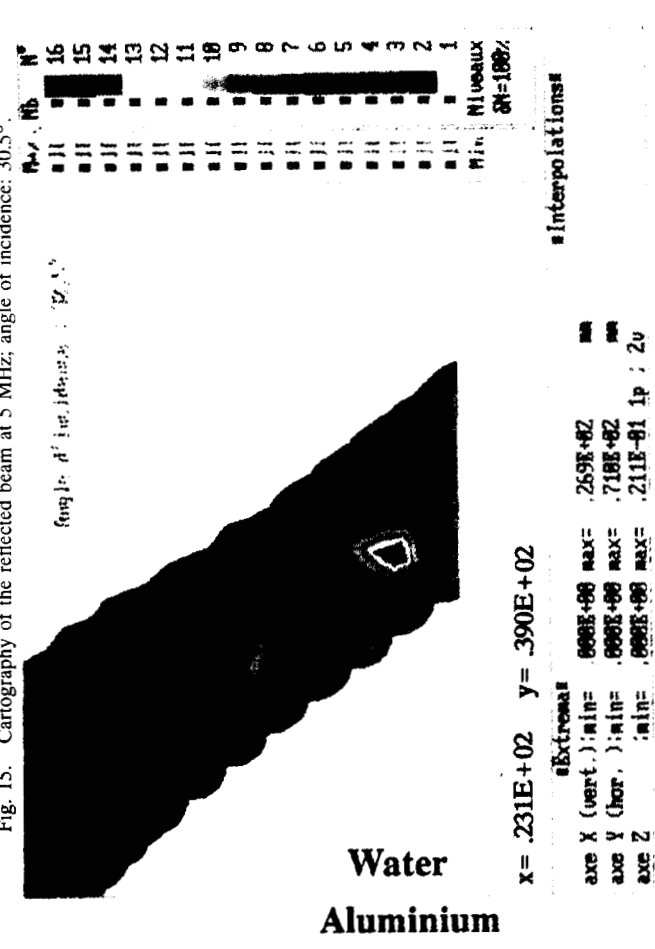


Fig. 17. Cartography of the reflected beam at 5 MHz; angle of incidence: 38°.

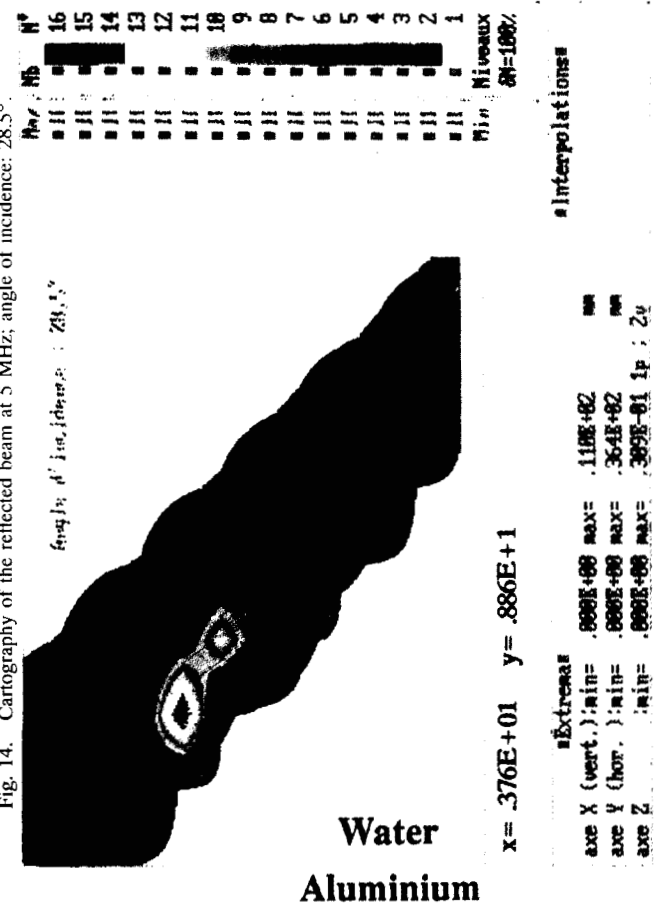


Fig. 16. Cartography of the reflected beam at 5 MHz; angle of incidence: 32.5°.

## REFERENCES

- [1] H. L. Bertoni, C. W. Hsue, and T. Tamir, "Non-specular reflection of convergent beams from liquid-solid interface," *Trait. Sign.*, vol. 2, no. 3, pp. 201-205, 1985.
- [2] P. B. Nagy, K. Cho, L. Adler, and D. E. Chimenti, "Focal shift of convergent ultrasonic beams reflected from a liquid-solid interface," *J. Acoust. Soc. Amer.*, vol. 81, no. 4, p. 835, Apr. 1987.
- [3] T. E. Matikas, M. Rousseau, and P. Gagniol, "Theoretical analysis for the reflection of a focused ultrasonic beam from a fluid-solid interface," submitted.
- [4] M. Rousseau and P. Gagniol, "Etude asymptotique d'un faisceau Gaussien focalise," *J. d'Acoust.*, vol. 1, pp. 95-99, 1988.
- [5] ———, "Short wave analysis for the reflection of bounded acoustic beams onto liquid-solid interfaces at the Rayleigh incidence," *J. Acoust. Soc. Amer.*, vol. 78, pp. 1859-1867, 1985.

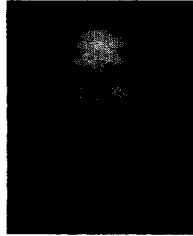


**Theodore E. Matikas** (S'89-M'91) received the Ph.D degree in mechanics of solids and structures in July 1991 from the University of Technology of Compiègne (UTC), France.

From 1988 to August 1991 he was a Research Fellow at the European Economic Community. He is now a National Research Council Research Associate at the Air Force Systems Command (AFSC), Air Force Wright Aeronautical Laboratories, Materials Directorate, Nondestructive Evaluation Branch, Wright-Patterson Air Force Base, OH.



**Martine Rousseau** is a Research Worker at the National Center of Scientific Research of France (CNRS) and works at the University of Paris in periodical media.



**Philippe Gagniol** is a Professor of physical acoustics at the University of Technology of Compiègne (UTC), France.